Scattering in step-index polymer optical fibers by side-illumination technique: theory and application

M. Asunción Illarramendi,* Gotzon Aldabaldetreku, Iñaki Bikandi, Joseba Zubia, Gaizka Durana, and Amaia Berganza

University of the Basque Country (UPV/EHU), ETSI de Bilbao, Alda. Urquijo s/n, E-48013 Bilbao, Spain
**Corresponding author: ma.illarramendi@ehu.es*

Received October 18, 2011; revised January 9, 2012; accepted January 9, 2012;
posted January 10, 2012 (Doc. ID 156786); published May 17, 2012

In this paper we present a detailed theoretical study that describes the generation of scattered light in step-index polymer optical fibers by using the side-illumination scattering measurement technique. A detailed analysis of the variation of the maximum angle of acceptance within the fiber has been carried out in order to calculate the scattered light as a function of different launching conditions. The theoretical model has been developed by using the Mie theory for spheres in the independent-scatterer approximation. © 2012 Optical Society of America

OCIS codes: 060.2270, 060.2310, 290.0290, 290.4020.

1. INTRODUCTION

Polymer optical fibers (POFs) have historically occupied a niche in the optical fiber world thanks to their robustness, large core diameters, high numerical apertures, and low cost [1,2]. Particularly, in the last few years POFs have been widely used both for short-haul communications links, where distances to cover are generally less than 1 km [3] and for a whole range of different sensing applications [4]. In fact, POFs have several advantages over their glass counterparts for fiber sensors, especially when microstructured fibers are used [5]. On the other hand, doped POFs have also raised a great interest in the field of fiber lasers, amplifiers and optical switches in the visible region [6–9]. The lower manufacturing temperatures of POFs as compared to glass fibers make it possible to embed a wide range of available materials into the fiber core.

Among several issues which affect the performance of POFs, limiting the maximum attainable distance and the information transmission capacity of an optical link, or compromising their sensitivity in sensing applications or decreasing the efficiency of the optical devices, is the scattering caused by the presence of inhomogeneities in the polymer [1]. The so-called Rayleigh scattering (for particles much smaller than the wavelength) is usually caused by subwavelength irregularities in the refractive index within the core of the fiber, whereas the Mie scattering (scatterers' size of the order of the wavelength) is due to inhomogeneities such as variations in the core-cladding refractive index, impurities at the core-cladding interface, strains or bubbles within the fiber core, or fluctuations in the fiber diameter. These types of effects are in large part responsible for the optical energy loss and the mode coupling in POFs [1,10,11]. For these reasons, light scattering has been an extensively investigated subject since the early days of POFs, with studies like those carried out by Koike *et al.* in [12] and [13] or, more recently by Bunge *et al.* in [14].

Scattering caused by inhomogeneities in the fiber can be analyzed by exciting the fiber transversally, that is, perpendicularly to the fiber axis. This type of excitation, which is called side-illumination technique, is used to characterize the optical losses in doped POFs or dye doped waveguides. Since this method is nondestructive, it constitutes an alternative technique to the traditional methods like the cutback method or the bulk measurement [9,15]. In case of nondoped fibers, this technique allows the measurement of the scattered light that is able to propagate through the fiber. Moreover, it has been demonstrated by previous works that the analysis of the dependence of the scattered light features on different launching conditions can give information about the size of the scattering centers and their position in the fiber [14,16].

In this study we have worked out a theoretical model in order to describe the dependence of the total amount of scattered light guided along a POF sample when it is transversally excited under different launching conditions. Unlike a previous work [14], the angular distribution of the scattered light has been described by the phase functions of the Mie theory for spheres. Scattering by a sphere of arbitrary size is called Mie scattering and it is an exactly solved phenomena. That is to say, we can use this theory to describe scattering generated by spheres of any size, from spheres much smaller than the wavelength of light (Rayleigh approximation) to spheres of larger size (geometrical optics limit). Besides the size of the inhomogeneity, the developed theory allows us to vary both the refractive index of the material of the scatterer and of the medium surrounding the scatterer, the wavelength of the incident radiation, and its polarization. In [14] calculations were performed in two optical ranges (Rayleigh and Mie limit) without indicating the exact size of the scatterer, the material in which the scatterer is made, or its surrounding material. On the other hand, the total amount of scattered intensity in [16] was obtained by applying the ray-tracing method on a fiber with a finite cladding, in contrast to the integration method used in [14] and in this work. The ray-tracing method, although approximate, has the advantage of allowing to obtain a complete description

of the scattered power distribution of rays at the output end of the fiber which is essential to calculate the numerical near- and far-fields patterns. In [16], the ray-tracing method was applied by describing the angular distribution of the scattered light from the Mie theory for spheres. However, due to paper length constraints, the theoretical modeling and its corresponding expressions were neither explained nor shown in that work. A very important feature of our analytical model is that it takes into account the accurate variation of the maximum angle of acceptance inside the fiber, showing that in some points near to the core-cladding interface the value of the critical angle becomes complex. This fact affects mainly the value of the scattered light intensity.

The paper is organized as follows. The theoretical model that describes the scattered light intensity as a function of different launching conditions is explained in detail through Section 2. The results obtained for several sizes and materials of the scattering centers and for different positions of the scattering centers within the fiber, are analyzed and discussed in Section 3. Finally, the summary of the work is presented in Section 4.

2. THEORETICAL MODELING

In the side-illumination technique, the light source inside the fiber is the scattered light generated when the fiber is illuminated from its lateral side. Figure 1 shows a schematic diagram of the side-illumination experiment for a multimode fiber. The geometry of scattering generation must be taken into account because the scattered light is not being measured in the same direction as the incident excitation. The scattered light intensity that reaches one of the fiber ends is going to be analyzed. The theoretical modeling has been done with the following assumptions: i) the scattered light is caused by inhomogeneities placed at the core-cladding interface and by inhomogeneities placed along the core fiber. These inhomogeneities are considered either as air bubbles or as cladding inlays on the assumption that the excess scattering in poly(methyl methacrylate) (PMMA) fibers is mainly caused by voids and core inclusions [2,13]. ii) Although in some cases many scattered sources are considered, for instance air bubbles placed at the core fiber, the effects of multiple scattering will be neglected. That is to say, the radiation to which each scatterer is exposed is essentially the light of the original beam [17]. iii) The scattering will be assumed to be independent, that is, the scatterers are sufficiently far from each other so that it is possible to study the scattering by one particle without reference to the other ones [17]. iv) The angular distribution of radiation generated by scatterers has been described from the Mie theory for spheres [17]. Scattering is characterized by two important numbers: the size parameter of the scattering particle (x) and the refractive index contrast (m). They are defined, respectively, as:

$$x = \frac{2\pi r}{\lambda} n_{\mathrm{sr}}, \qquad m = \frac{n_{\mathrm{scatt}}}{n_{\mathrm{sr}}}, \tag{1}$$

where r is the radius of the sphere and n_{scatt} and n_{sr} are the refractive indexes of the scattering center and the medium surrounding it. λ is the wavelength of the incident radiation. v) The scatterers have been assumed spherical particles, that is, the nonspherical scatterer has been replaced by an area equivalent sphere with a radius (r) which represents the half of the averaged mean scatterer size (ϕ). Although polarization effects depend on the particle shape, the nonspherical/spherical differences are expected to be small when the value of the size parameter $x \cong 10$ [18]. vi) The effects of the cladding thickness in the fibers have been neglected. Therefore, it has been assumed the same value for the total fiber radius and the core radius (ρ_{core}). vii) The light detected at any of the ends of the step-index polymer fiber is the scattered light lying within the maximum angle of acceptance (or critical angle) of the fiber and it includes both guided and leaky (tunneling) rays. In general, tunneling rays have larger losses than the guided rays and

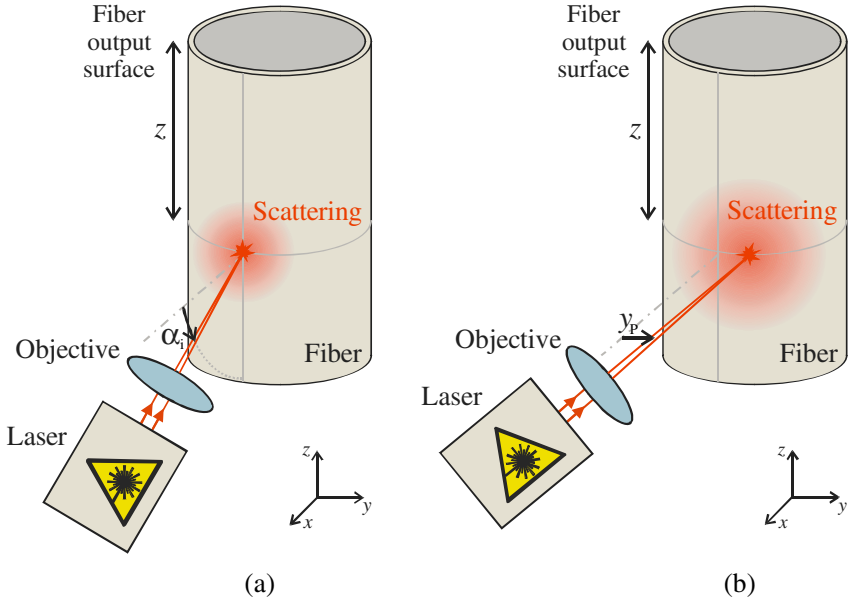

Fig. 1. (Color online) Scattering generated in a fiber with a monochromatic laser beam by side-illumination technique. The scattered light that propagates a distance z within the fiber to one of the fiber ends is detected. (a) Angular scan. α_i is the angle made by the incident beam with the normal to the fiber surface at $y = 0$ μm. The incident beam always lies in the xy-plane. (b) Lateral scan. y_P refers to the y-coordinate of the point of incidence relative to $y = 0$ μm. The incident beam always lies in the xy-plane (parallel to the x-axis).

they are usually treated as rays as in the cutoff condition. However, in short distances the tunneling rays may not attenuate sufficiently [11]. Since our fibers are extremely short (about 20 cm), we will assume that the propagation losses of both modes (guided and leaky) are equal and negligible.

Two different launching conditions have been analyzed. In the first one, the light is focused on the fiber axis with the incident plane containing the fiber axis and the angle of incidence is varied (*angular dependence*) [see Fig. 1(a)]. In the second one, the direction of the incident light is fixed with an incident plane perpendicular to the fiber axis and, now, it is the position of the incident spot what actually varies (*lateral dependence*) [see Fig. 1(b)].

A. Angular Dependence

The geometrical arrangement corresponding to this incidence together with the definition of the angles used for the theoretical analysis are described in Appendix A. In order to obtain the scattered light that will be detected at one of the ends of the fiber we must first calculate the maximum acceptance angle of the fiber for a scattered beam. This maximum acceptance angle is, in most cases, different to the well-known critical angle defined for guided rays, since the sources of the detected light are scattering centers placed in any position inside the fiber. In Appendix A, we provide a detailed procedure for calculating the maximum angle of acceptance corresponding to this incidence. In general, the maximum acceptance angle of the fiber $(\theta_z)_c$ [see Eq. (A9)] depends on two variables: the location x_Q of the point source along the refracted beam and the angle ϕ_x of the scattered beam relative to the x-axis in the xy-plane. When the scattered light is produced by a scatterer placed just in the cladding-core interface, it only depends on the angle ϕ_x [see Eq. (A10)]. Notice that there is no dependence of $(\theta_z)_c$ on the incident angle α_i.

If the scattered light were produced from one scatterer placed at the center of the fiber, x_Q would be zero and thus the critical angle would only depend on the refractive indexes of the core and the cladding. In this case, the critical angle is given by the expression defined for guided rays [11], that is:

$$\sin(\theta_z)_c(0,\phi_x) = \sqrt{1-\left(\frac{n_{\text{clad}}}{n_{\text{core}}}\right)^2} = \sqrt{1-n^2}, \tag{2}$$

where n represents the quotient $n_{\text{clad}}/n_{\text{core}}$. n_{core} and n_{clad} are, respectively, the refractive indexes of the fiber core and the fiber cladding. The fact that the maximum acceptance angle calculated for any scattered beam [Eq. (A9)] is higher than that obtained from Eq. (2) indicates that both guided and leaky (tunneling) rays are excited by the scatterers illuminated by the refracted beam [19]. Notice that the angle θ_z (the angle taken by the scattered beam with respect to the fiber axis) must satisfy the condition $0 \le \theta_z < \arcsin(\sqrt{1-n^2})$, so that the rays generated in the fiber are guided [11].

If one analyzes the expressions obtained for $\sin(\theta_z)_c$ [Eqs. (A9) and (A10)], it is concluded that the variables x_Q and ϕ_x are not allowed to vary in their entire ranges, (i.e., $-\rho_{\text{core}} \le x_Q \le \rho_{\text{core}}$ and $0 \le \phi_x \le 2\pi$). More specifically, in order to obtain real-valued arguments for the sine function in Eq. (A9), we must impose the constraint that the critical angle does not exceed $\pi/2$. That is, it is required that x_Q and ϕ_x satisfy the following relation:

$$1 > n^2 \ge \left(\frac{x_Q}{\rho_{\text{core}}}\sin\phi_x\right)^2$$
$$\text{for } \sin(\theta_z)_c(x_Q,\phi_x) = \frac{\sqrt{1-n^2}}{\sqrt{1-\left(\frac{x_Q}{\rho_{\text{core}}}\sin\phi_x\right)^2}}. \tag{3}$$

Equation (3) defines a valid region for guided and tunneling rays arisen from the scatterers in terms of the scatterer position (x_Q) and the scattered direction (ϕ_x). As an example, Fig. 2 shows two contour plots of $\sin(\theta_z)_c$ as a function of both x_Q and ϕ_x corresponding to two step-index plastic optical fibers with the same core material and radius ($n_{\text{core}} = 1.49$ and $\rho_{\text{core}} = 490\ \mu$m) but with different cladding material ($n_{\text{clad}} = 1.4036$ or $n_{\text{clad}} = 1$). It can be seen that the curves are symmetrical with respect to $x_Q = 0$ and $\phi_x = \pi$ and that at some source points (near to the fiber interfaces) there is scattering light in certain specific directions whose the maximum acceptance angle is not defined, i.e., no scattered light is directed to the fiber endface. For instance, were ϕ_x allowed to vary throughout its entire range, (i.e., from 0 to 2π), x_Q should vary only in the range given by $-\rho_{\text{core}}n \le x_Q \le \rho_{\text{core}}n$. For

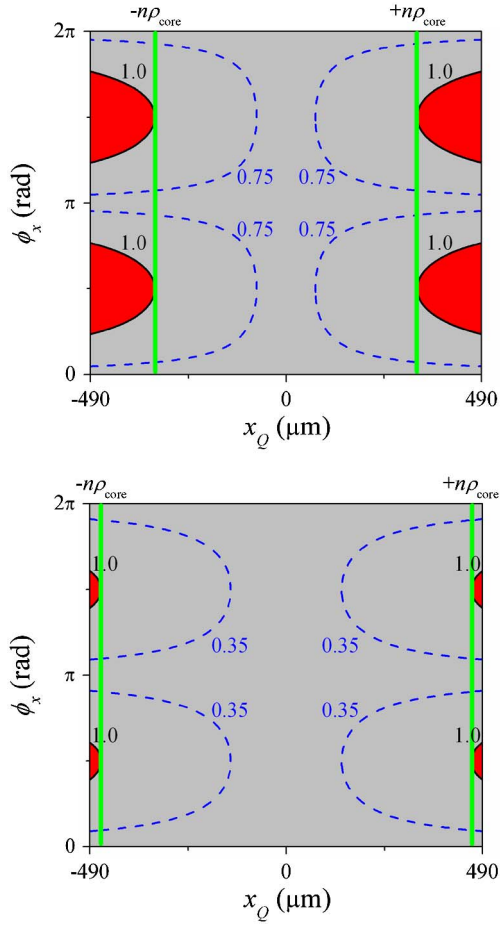

Fig. 2. (Color online) Contour plots of $\sin(\theta_z)_c$ as a function of both x_Q and ϕ_x corresponding to two fibers with the same core material, $n_{\text{core}} = 1.49$ and radius $\rho_{\text{core}} = 490\ \mu$m, but different cladding material. Black solid lines correspond to $\sin(\theta_z)_c = \pm 1$ and green solid ones $x_Q = \pm n\rho_{\text{core}}$. Red painted areas indicate the forbidden region for x_Q and ϕ_x giving no real critical angle. (Top plot) $n_{\text{clad}} = 1$. Blue dashed lines correspond to $\sin(\theta_z)_c = \pm 0.75$. (Bottom plot) $n_{\text{clad}} = 1.4036$. Blue dashed lines correspond to $\sin(\theta_z)_c = \pm 0.35$.

scatterers placed at the core-cladding interface, (that is, $x_Q = \rho_{\text{core}}$), ϕ_x is only allowed to vary in the following ranges: $0 \le \phi_x \le \arcsin(n)$, $\pi - \arcsin(n) \le \phi_x \le \arcsin(n) + \pi$, and $2\pi - \arcsin(n) \le \phi_x \le 2\pi$. It can be also noticed that, as the quotient n approaches the value 1, the forbidden regions, where the $(\theta_z)_c$ angle is not defined, become smaller and, consequently, the effects of the truncation of the critical angle will not be very significant. The scattered beams emerging close to the cladding-core interface which give imaginary values for the critical angle can be interpreted as nonpropagating or evanescent modes along the fiber axis. These modes describe the energy stored in the immediate vicinity of fiber discontinuities [11]. The imposition that the critical angle cannot exceed $\pi/2$ and its effects on the near field patterns of step-index fibers have been reported in [19].

Let us now calculate the fraction of the scattered intensity within the critical angle that will propagate along the fiber as a function of the incident angle. The radiation pattern of the scattered light produced by centers placed at any point along the path covered by the refracting beam inside the fiber is given by the Mie theory for spheres. The intensity of the scattered light in an arbitrary direction is given by means of a dimensionless function, $F(\theta_{\text{IS}}, \phi_{\text{PS}})$ [17]:

$$F(\theta_{\text{IS}}, \phi_{\text{PS}}) = [|S_1(\theta_{\text{IS}})|^2 \sin^2 \phi_{\text{PS}} + |S_2(\theta_{\text{IS}})|^2 \cos^2 \phi_{\text{PS}}]. \quad (4)$$

S_1 and S_2 are the Mie phase functions and they depend on the angle between the scattered beam and the incident beam on the scatterer (θ_{IS}). The input parameters required to calculate these functions are the wavelength of the incident electromagnetic radiation (λ), the radius of the scattering sphere, and its refractive index contrast (m). ϕ_{PS} is the angle between the electric field of the incident light on the scatterer and the scattering plane, (the plane formed by the incident and scattered beams). It must be taken into account that in the description of the scattering process given by Eq. (4), the incident beam is the light which impinges on the scatterer. Therefore, if the scatterer is placed at the core-cladding interface the incident beam impinging on the scatterer is the incident beam (**i**), whereas if it is placed within the core the incident beam turns out to be the refracted one (**r**) (see Fig. 15 in Appendix A). The expressions for θ_{IS} and ϕ_{PS} as a function of θ_z and ϕ_x and for the two polarizations analyzed (see Appendix A) have been worked out and they can be found in Table 1.

Therefore, the dependence on the incident angle of the scattered light intensity generated by scatterers placed along the refracting beam within the core for both polarizations $I_{\text{TE,TM}}(\alpha_i)$ would be proportional to the integral:

$$\begin{aligned} I_{\text{TE,TM}}(\alpha_i) \propto T_{\text{TE,TM}}(\alpha_i) \Bigg[& 2 \int_0^{\arcsin(n)} d\phi_x \int_{-\rho_{\text{core}}}^{\rho_{\text{core}}} \frac{dx_Q}{\cos \alpha_r} \\ & \times \int_0^{(\theta_z)_c(x_Q,\phi_x)} F(\theta_z, \phi_x)|_{\text{TE,TM}} \sin \theta_z d\theta_z \\ & + 2 \int_{\pi-\arcsin(n)}^{\pi} d\phi_x \int_{-\rho_{\text{core}}}^{\rho_{\text{core}}} \frac{dx_Q}{\cos \alpha_r} \\ & \times \int_0^{(\theta_z)_c(x_Q,\phi_x)} F(\theta_z, \phi_x)|_{\text{TE,TM}} \sin \theta_z d\theta_z \\ & + 2 \int_{\arcsin(n)}^{\pi-\arcsin(n)} d\phi_x \int_{-n\rho_{\text{core}}/\sin\phi_x}^{+n\rho_{\text{core}}/\sin\phi_x} \frac{dx_Q}{\cos \alpha_r} \\ & \times \int_0^{(\theta_z)_c(x_Q,\phi_x)} F(\theta_z, \phi_x)|_{\text{TE,TM}} \sin \theta_z d\theta_z \Bigg], \end{aligned} \quad (5)$$

where $T_{\text{TE,TM}}$ denotes the Fresnel's coefficients given by either Eq. (A3) or (A4) and $(\theta_z)_c$ is given by Eq. (A9). The integrals over x_Q and ϕ_x have been evaluated taking into account the restrictions for the critical angle commented before. The length traveled by the refracting beam has been taken as the distance x_Q divided by $\cos \alpha_r$. The propagation losses of the scattered light (guided and tunneling rays) and the absorption of the refracted beam inside the fiber have been neglected on the basis of the short lengths involved.

If the scattered intensity would be generated from one scattering center placed at the core-cladding interface ($x_Q = \rho_{\text{core}}$) the dependence of the intensity on α_i would be given by the integral:

$$\begin{aligned} I_{\text{TE,TM}}(\alpha_i) \propto T_{\text{TE,TM}}(\alpha_i) \Bigg[& 2 \int_0^{\arcsin(n)} d\phi_x \\ & \times \int_0^{(\theta_z)_c(\rho_{\text{core}},\phi_x)} F(\theta_z, \phi_x)|_{\text{TE,TM}} \sin \theta_z d\theta_z d\phi_x \\ & + 2 \int_{\pi-\arcsin(n)}^{\pi} d\phi_x \\ & \times \int_0^{(\theta_z)_c(\rho_{\text{core}},\phi_x)} F(\theta_z, \phi_x)|_{\text{TE,TM}} \sin \theta_z d\theta_z d\phi_x \Bigg], \end{aligned} \quad (6)$$

with $(\theta_z)_c$ given by Eq. (A10).

B. Lateral Dependence

The geometrical arrangement corresponding to this incidence, the variables used for the optical analysis, and the procedure for calculating the critical angle in this case are provided in Appendix B. The obtained expression of the maximum acceptance angle $(\theta_z)_c$ [see Eq. (B7)] depends now on three variables: x'_Q, the position of the scatterer along

Table 1. Principal Expressions Used in the Theoretical Calculations of the Scattered Intensity as a Function of the Incident Angle (α_i)[a]

	Angular Dependence($\lvert x_Q \rvert < \rho_{\text{core}}$)	Angular Dependence($x_Q = \rho_{\text{core}}$)
$\sin(\theta_z)_c$	$\sin(\theta_z)_c(x_Q, \phi_x) = \frac{\sqrt{1-n^2}}{\sqrt{1-(\frac{x_Q}{\rho_{\text{core}}} \sin \phi_x)^2}}$	$\sin(\theta_z)_c(\rho_{\text{core}}, \phi_x) = \frac{\sqrt{1-n^2}}{\cos \phi_x}$
$\cos \theta_{\text{IS}}$	$-\cos \alpha_r \sin \theta_z \cos \phi_x + \sin \alpha_r \cos \theta_z$	$-\cos \alpha_i \sin \theta_z \cos \phi_x + \sin \alpha_i \cos \theta_z$
$(\sin \phi_{\text{PS}})_{\text{TM}}$	$\frac{-\sin \theta_z \sin \phi_x}{\sqrt{(\sin \theta_z \sin \phi_x)^2 + (\sin \alpha_r \sin \theta_z \cos \phi_x + \cos \alpha_r \cos \theta_z)^2}}$	$\frac{-\sin \theta_z \sin \phi_x}{\sqrt{(\sin \theta_z \sin \phi_x)^2 + (\sin \alpha_i \sin \theta_z \cos \phi_x + \cos \alpha_i \cos \theta_z)^2}}$
$(\sin \phi_{\text{PS}})_{\text{TE}}$	$\frac{\cos \alpha_r \cos \theta_z + \sin \alpha_r \sin \theta_z \cos \phi_x}{\sqrt{(\sin \theta_z \sin \phi_x)^2 + (\sin \alpha_r \sin \theta_z \cos \phi_x + \cos \alpha_r \cos \theta_z)^2}}$	$\frac{\cos \alpha_i \cos \theta_z + \sin \alpha_i \sin \theta_z \cos \phi_x}{\sqrt{(\sin \theta_z \sin \phi_x)^2 + (\sin \alpha_i \sin \theta_z \cos \phi_x + \cos \alpha_i \cos \theta_z)^2}}$
$(\mathbf{E})_{\text{TM}}$	$\mathbf{E}_i = -E_0(\sin \alpha_i \mathbf{x} + \cos \alpha_i \mathbf{z})$; $\mathbf{E}_r = -E_0(\sin \alpha_r \mathbf{x} + \cos \alpha_r \mathbf{z})$	$\mathbf{E}_i = -E_0(\sin \alpha_i \mathbf{x} + \cos \alpha_i \mathbf{z})$
$(\mathbf{E})_{\text{TE}}$	$\mathbf{E}_i = E_0\mathbf{y}$; $\mathbf{E}_r = E_0\mathbf{y}$	$\mathbf{E}_i = E_0\mathbf{y}$

[a]Two particular cases have been distinguished: scatterers placed within the core ($\lvert x_Q \rvert < \rho_{\text{core}}$) and one scatterer at the core-cladding interface ($x_Q = \rho_{\text{core}}$). $\mathbf{E}_i$ and $\mathbf{E}_r$ are the electric fields of the incident and refracted beams, respectively.

the refracting beam (x'-axis); ϕ_x, the angle of the scattered beam relative to the x-axis in the xy-plane; and, y_P, the height of the incident point on the fiber. It can be seen that the value of $(\theta_z)_c$ is higher than the value corresponding to the guided rays [Eq. (2)] indicating that both guided and tunneling rays are included in our analysis.

The constrain that the critical angle does not exceed $\pi/2$ implies that the following relation must be satisfied for $(\theta_z)_c$:

$$1 > n^2 \geq \frac{(x'_Q)^2 + \left(\frac{y_P}{n_{\text{core}}}\right)^2}{\rho_{\text{core}}^2} \sin^2\left[\phi_x + \arctan\left(\frac{y_P}{n_{\text{core}} x'_Q}\right) + \arctan\left(\frac{y_P}{\sqrt{\rho_{\text{core}}^2 - y_P^2}}\right) - \arcsin\left(\frac{y_P}{\rho_{\text{core}} n_{\text{core}}}\right)\right]. \quad (7)$$

For a scattering center placed at the core-cladding interface [Eq. (B8)], the condition is simplified to the next relation:

$$1 > n^2 \geq \sin^2\left[\phi_x + \arctan\left(\frac{y_P}{\sqrt{\rho_{\text{core}}^2 - y_P^2}}\right)\right]. \quad (8)$$

As we commented before, the restrictions in the value of the sine function [Eq. (7) and Eq. (8)] in terms of the scatterer position (x'_Q), the direction of the scattered beam (ϕ_x) and the lateral height (y_P) define a valid region for guided and tunneling rays within the fiber. For instance, we can see in Fig. 3 the contour plot of $\sin(\theta_z)_c(\phi_x, y_P)$ for a scattering center placed at the core-cladding interface as a function of ϕ_x and y_P [Eq. (B8)]. The results correspond to a commercial step-index POF fiber with $n_{\text{core}} = 1.49$, $n_{\text{clad}} = 1.4036$, and $\rho_{\text{core}} = 490$ μm. We can observe again that there are forbidden regions corresponding to specific values of ϕ_x and y_P where the maximum acceptance angle is not defined. The modes associated to these regions can be interpreted as non-propagating modes whose energy is stored close to fiber discontinuities [11].

The dependence on the lateral height of the scattered light intensity for the two polarizations analyzed (see Appendix B) is proportional to the following expression:

$$I_{\text{TE,TM}}(y_P) \propto T_{\text{TE,TM}}(y_P) \int_R \mathrm{d}x'_Q \int_R \mathrm{d}\phi_x \times \int_0^{(\theta_z)_c(x'_Q,\phi_x,y_P)} F(\theta_z, \phi_x)|_{\text{TE,TM}} \sin\theta_z \mathrm{d}\theta_z. \quad (9)$$

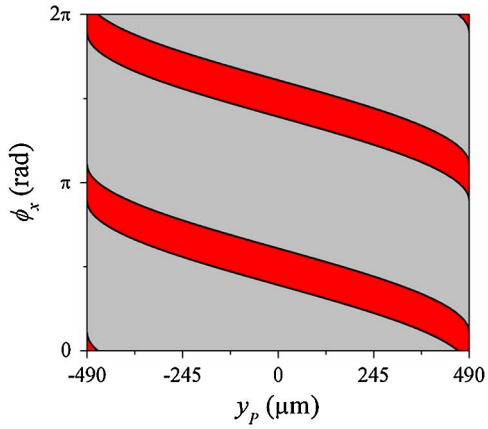

Fig. 3. (Color online) Contour plots of $\sin(\theta_z)_c$ for a scattering center placed at the core-cladding interface [Eq. (25)] as a function of both y_P and ϕ_x corresponding to a fiber with $n_{\text{core}} = 1.49$, $n_{\text{clad}} = 1.4036$, and $\rho_{\text{core}} = 490$ μm. Black solid lines correspond to the limit $\sin(\theta_z)_c = \pm 1$. Filled areas indicate the range of values of y_P and ϕ_x leading to no real critical angle.

The integrals over x'_Q and ϕ_x should be evaluated in the region R where the maximum acceptance angle is real-valued. $T_{\text{TE,TM}}$ denotes the Fresnel's coefficients given by either Eq. (B3) or (B4). The radiation pattern of the scattered light in an arbitrary direction given by $F(\theta_{\text{IS}}, \phi_{\text{PS}})$, has been worked out again using the corresponding expressions for the angles θ_{IS} and ϕ_{PS}. The expressions have been summarized in Tables 2 and 3 for scatterers placed within the core or at the core-cladding interface, respectively. Notice that the factor $\cos\alpha_r$ has not been included in the integral because the refracted beam is traveling along the direction of x'-axis in the xy-plane. The propagation losses and the absorption of the refracted beam inside the fiber have neither been taken into account. If the scattering center is placed at the core-cladding interface ($\rho_{\text{core}} = \sqrt{x_Q^2 + y_Q^2} = \sqrt{x_Q'^2 + y_Q'^2}$), the dependence would be given by:

$$I_{\text{TE,TM}}(y_P) \propto T_{\text{TM,TE}}(y_P) \int_R \mathrm{d}\phi_x \int_0^{(\theta_z)_c(\phi_x,y_P)} F(\theta_z, \phi_x)|_{\text{TM,TE}} \times \sin\theta_z \mathrm{d}\theta_z, \quad (10)$$

where the angle integral should not be evaluated from 0 to 2π but in the region R where Eq. (8) is satisfied, that is, in the followings ranges (see also Fig. 3):

$$-\arcsin(n) - \arctan\left(\frac{y_P}{\sqrt{\rho_{\text{core}}^2 - y_P^2}}\right) \quad \text{or} \quad 0 \leq \phi_x \leq \arcsin(n) - \arctan\left(\frac{y_P}{\sqrt{\rho_{\text{core}}^2 - y_P^2}}\right),$$

$$-\arcsin(n) - \arctan\left(\frac{y_P}{\sqrt{\rho_{\text{core}}^2 - y_P^2}}\right) + \pi \leq \phi_x \leq \arcsin(n) - \arctan\left(\frac{y_P}{\sqrt{\rho_{\text{core}}^2 - y_P^2}}\right) + \pi,$$

$$-\arcsin(n) - \arctan\left(\frac{y_P}{\sqrt{\rho_{\text{core}}^2 - y_P^2}}\right) + 2\pi \leq \phi_x \leq \arcsin(n) - \arctan\left(\frac{y_P}{\sqrt{\rho_{\text{core}}^2 - y_P^2}}\right) + 2\pi \quad \text{or} \quad 2\pi. \quad (11)$$

Table 2. Principal Equations Used in the Theoretical Calculations of the Scattered Intensity from Scatterers Placed within the Core as a Function of Incident Lateral Height (y_P)[a]

	Lateral Dependence
$\sin(\theta_z)_c(x'_Q, \phi_x, y_P)$	$\frac{\sqrt{1-n^2}}{\sqrt{1-\frac{(x'_Q)^2+\left(\frac{y_P}{n_{\text{core}}}\right)^2}{\rho_{\text{core}}^2}\sin^2\left[\phi_x+\arctan\left(\frac{y_P}{n_{\text{core}}x'_Q}\right)+\arctan\left(\frac{y_P}{\sqrt{\rho_{\text{core}}^2-y_P^2}}\right)-\arcsin\left(\frac{y_P}{\rho_{\text{core}}n_{\text{core}}}\right)\right]}}$
$\sin(\theta_z)_c(x'_Q, \phi_x, 0) y_P = 0$	$\frac{\sqrt{1-n^2}}{\sqrt{1-\left(\frac{x'_Q}{\rho_{\text{core}}}\sin\phi_x\right)^2}}$
$\cos\theta_{\text{IS}}$	$-\sin\theta_z\,\cos(\phi_x+\alpha_i-\alpha_r)$
$(\sin\phi_{\text{PS}})_{\text{TM}}$	$\frac{\cos\theta_z}{\sqrt{(\sin\theta_z\,\sin(\phi_x+\alpha_i-\alpha_r))^2+(\cos\theta_z)^2}}$
$(\sin\phi_{\text{PS}})_{\text{TE}}$	$\frac{\sin\theta_z\,\sin(\phi_x+\alpha_i-\alpha_r)}{\sqrt{(\sin\theta_z\,\sin(\phi_x+\alpha_i-\alpha_r))^2+(\cos\theta_z)^2}}$
$(\mathbf{E})_{\text{TM}}$	$\mathbf{E}_i = E_0\mathbf{y};\ \mathbf{E}_r = E_0[-\sin(\alpha_i-\alpha_r)\mathbf{x}+\cos(\alpha_i-\alpha_r)\mathbf{y}]$
$(\mathbf{E})_{\text{TE}}$	$\mathbf{E}_i = E_0\mathbf{z};\ \mathbf{E}_r = E_0\mathbf{z}$

[a]$\mathbf{E}_i$ and $\mathbf{E}_r$ are the electric fields of the incident and refracted beams, respectively.

The complete analytical expressions corresponding to the angular distribution in the Mie theory for spheres, $F(\theta_{\text{IS}}, \phi_{\text{PS}})$, are very intricate [17]. However, in the Rayleigh limit these expressions are much simpler and, in addition, they can be easily obtained. According to this limit, the angular distribution of the scattered wave is proportional to the square of the sine function of the angle between the scattering direction (**s**) and the polarization of the incident beam [20]. The expressions obtained for the angular distributions in this limit for both launching conditions and both polarizations are shown in Table 4.

3. DISCUSSION

Let us analyze the potential of the theory described just above in order to characterize the scattering in step-index POFs. As we show below, our analytical expressions describe the variations observed in the curves of the scattered intensity as a function of the incident angle and the lateral height ($I(\alpha_i)$ and $I(y_P)$ curves) as the scatterer size increases. These effects, which have been shown in [14,16] for the case of air scattering centers, can be summarized as follows: an increase of the value of the scattered intensity, a diminution of the differences between the curves of the scattered intensity [$I(\alpha_i)$ and $I(y_P)$ curves] corresponding to each polarization, a change in the shape of the $I(\alpha_i)$ curves (from symmetric to asymmetric form) and the emergence of two peaks in the boundaries of the core-cladding interface in the $I(y_P)$ curves. These behaviors can be easily explained taking into account the shapes of the Rayleigh and Mie scattering angular distributions [17,20,21]. However, if we take into account that the theory allows to select besides the size, the material of the scatterer, and the material surrounding the scatterer, we can take a step forward and study, for example, the variations that occur in the scattered intensity curves simply by changing the material in which the scattering sphere is made, in particular from an air inhomogeneity to a fiber cladding material one. Air and cladding material inclusions within the fiber are some of the main sources of the excess scattering in POFs [2,13] and their effect is clearly distinguishable in the variations of the scattered light, since such variations are closely related to the refractive index contrast ($m = n_{\text{scatt}}/n_{\text{sr}}$). We may have chosen another material for the scattering center embedded in the fiber (like one based on residual monomers of PMMA) but this option would give a refractive index contrast very similar to that corresponding to the cladding material and, consequently, the differences between both scattered intensity curves would not be very significant.

Table 3. Principal Equations Used in the Theoretical Calculations of the Scattered Intensity from One Scatterer at the Core-Cladding Interface ($\rho_{\text{core}} = \sqrt{x_Q^2+y_Q^2} = \sqrt{x_P^2+y_P^2}$) as a Function of Incident Lateral Height (y_P)[a]

	Lateral Dependence ($\rho_{\text{core}} = \sqrt{x_Q^2+y_Q^2} = \sqrt{x_P^2+y_P^2}$)
$\sin(\theta_z)_c(\phi_x, y_P)$	$\frac{\sqrt{1-n^2}}{\cos\left[\phi_x+\arctan\left(\frac{y_P}{\sqrt{\rho_{\text{core}}^2-y_P^2}}\right)\right]}$
$\sin(\theta_z)_c(\phi_x)\ y_P = 0$	$\frac{\sqrt{1-n^2}}{\cos\phi_x}$
$\cos\theta_{\text{IS}}$	$-\sin\theta_z\,\cos\phi_x$
$(\sin\phi_{\text{PS}})_{\text{TM}}$	$\frac{\cos\theta_z}{\sqrt{(\sin\theta_z\,\sin\phi_x)^2+(\cos\theta_z)^2}}$
$(\sin\phi_{\text{PS}})_{\text{TE}}$	$\frac{\sin\theta_z\,\sin\phi_x}{\sqrt{(\sin\theta_z\,\sin\phi_x)^2+(\cos\theta_z)^2}}$
$(\mathbf{E})_{\text{TM}}$	$\mathbf{E}_i = E_0\mathbf{y}$
$(\mathbf{E})_{\text{TE}}$	$\mathbf{E}_i = E_0\mathbf{z}$

[a]$\mathbf{E}_i$ is the electric field of the incident beam.

For the reasons given above, we have first investigated the scattered light by air and fiber cladding spheres of different sizes placed at the core-cladding interface with an incident radiation $\lambda = 633$ nm. The sizes analyzed, from $\phi = 10$ nm to $\phi = 2000$ nm, correspond approximately to two important ranges: Rayleigh scattering ($\phi \ll \lambda$, $x \ll 1$) and Mie scattering ($\phi \approx \lambda$). These scattering regimes are depicted in Fig. 4. In this figure the scattering quality factor Q_s (the scattering cross-section normalized by the geometrical cross-section) [17] is plotted as a function of the particle size. The results correspond to an air sphere enclosed by core material ($m = 1/n_{\text{core}}$) and to a cladding sphere surrounded by core material ($m = n_{\text{clad}}/n_{\text{core}}$) for an incident radiation of $\lambda = 633$ nm. It can be seen that the scattering quality factor and, consequently, the scattered intensity, is always higher in the case of air sphere for the range of sizes analyzed (10 nm–2000 nm). Notice that this fact is not satisfied at other

Table 4. Expressions Obtained for the Angular Distribution Function $F(\theta_z,\phi_x)$ in the Rayleigh Approximation for Two Launching Conditions and Two Polarizations[a]

	Angular Dependence
$(F(\theta_z,\phi_x))_{\mathrm{TE}}$ $\lvert x_Q\rvert < \rho_{\mathrm{core}}$	$\cos^2\theta_z + \sin^2\theta_z\cos^2\phi_x$
$(F(\theta_z,\phi_x))_{\mathrm{TM}}$ $\lvert x_Q\rvert < \rho_{\mathrm{core}}$	$\sin^2\theta_z(1-\cos^2\phi_x\sin^2\alpha_r)+\cos^2\theta_z\sin^2\alpha_r-\frac{1}{2}\sin 2\alpha_r\sin 2\theta_z\cos\phi_x$
$(F(\theta_z,\phi_x))_{\mathrm{TE}}$ $x_Q=\rho_{\mathrm{core}}$	$\cos^2\theta_z + \sin^2\theta_z\cos^2\phi_x$
$(F(\theta_z,\phi_x))_{\mathrm{TM}}$ $x_Q=\rho_{\mathrm{core}}$	$\sin^2\theta_z(1-\cos^2\phi_x\sin^2\alpha_i)+\cos^2\theta_z\sin^2\alpha_i-\frac{1}{2}\sin 2\alpha_i\sin 2\theta_z\cos\phi_x$
	Lateral Dependence
$(F(\theta_z,\phi_x))_{\mathrm{TE}}$ $\lvert x_Q\rvert < \rho_{\mathrm{core}}$	$\sin^2\theta_z$
$(F(\theta_z,\phi_x))_{\mathrm{TM}}$ $\lvert x_Q\rvert < \rho_{\mathrm{core}}$	$\cos^2\theta_z + \sin^2\theta_z\cos^2(\phi_x+\alpha_r-\alpha_i)$
$(F(\theta_z,\phi_x))_{\mathrm{TE}}$ $x_Q=\rho_{\mathrm{core}}$	$\sin^2\theta_z$
$(F(\theta_z,\phi_x))_{\mathrm{TM}}$ $x_Q=\rho_{\mathrm{core}}$	$\cos^2\theta_z + \sin^2\theta_z\cos^2\phi_x$

[a]Two particular cases have been distinguished: scatterers within the core ($\lvert x_Q\rvert < \rho_{\mathrm{core}}$) and one scatterer at the core-cladding interface ($x_Q=\rho_{\mathrm{core}}$).

ranges of sizes. The $I(\alpha_i)$ and $I(y_P)$ curves generated by one air scatterer and by one cladding scatterer of three different sizes are plotted in Figs. 5, 6, 7, and 8. The scatterers are placed at the core-cladding interface and are surrounded by core material. The values of refractive indexes of the core and cladding fiber and the radius fiber used in the calculations correspond to a commercial step-index POF. By comparing the scattering curves obtained for one air sphere with those obtained for the cladding one, we observe that the scattered light from an air sphere is about one order of magnitude higher than that scattered by a cladding sphere for the same value of the scatterer size. This agrees with the calculation of the scattering quality factor Q_s shown in Fig. 4. As it can be seen in Figs. 5 and 6, at smallest sizes (from 10 nm to 300 nm) the shape of the $I(\alpha_i)$ curves corresponding to $m=1/n_{\mathrm{core}}$ and those calculated with $m=n_{\mathrm{clad}}/n_{\mathrm{core}}$ is similar. The quotient between the curves calculated with an air sphere and those calculated with a cladding one is around three. However, at larger sizes, the variation of the intensity in the range of the positive angles becomes less pronounced in the curve corresponding to a cladding sphere [see Figs. 5(c) and 6(c)]. Analogous behavior is observed in the lateral dependence curves. There are practically no differences between the shapes of the $I(y_P)$ curves obtained for the air and the cladding scatterer in the range of sizes from $\phi=10$ nm to $\phi=300$ nm, but at larger scatterer sizes, noticeable dissimilarities between the $I(y_P)$ curves are perceived [see Figs. 7(b), (c) and Figs. 8(b), (c)].

A simple comparison between these theoretical simulations and the experimentally determined curves corresponding to the same commercial POF (Figs. 4 and 5 of [16]), suggests us that the mean size of the scatterer that gives rise to the experimental scattering curves is at least 200 nm and that the predominant inhomogeneity is a cladding scatterer. As we

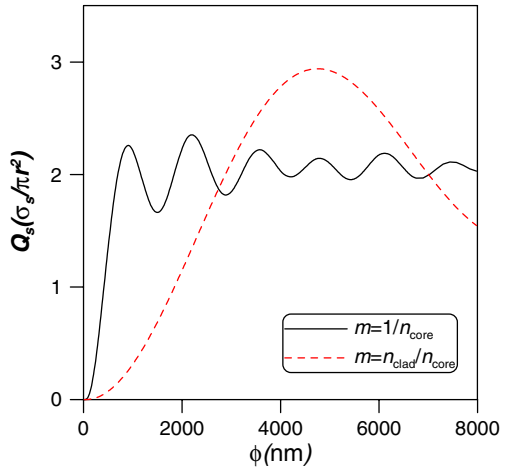

Fig. 4. (Color online) Scattering quality factor plotted versus the particle size of an air sphere (solid line) and a cladding sphere (dashed line) enclosed by core material for a radiation of wavelength $\lambda=633$ nm. For $\phi\gg\lambda$ (geometrical optics limit) both scattering quality factors converge to 2.

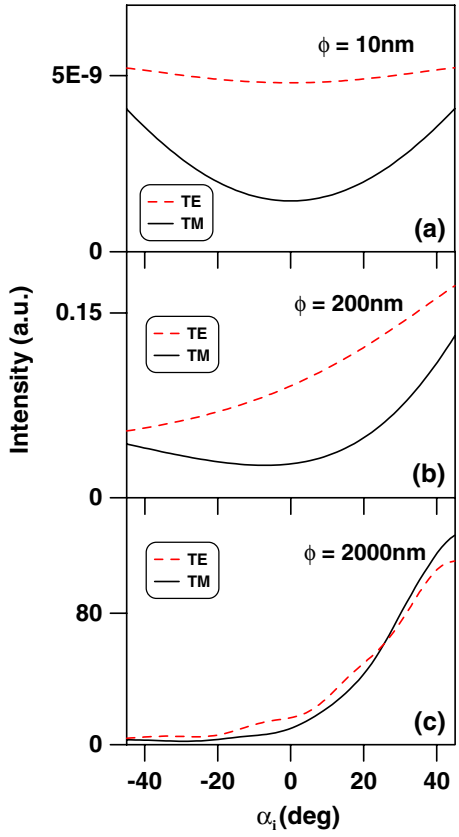

Fig. 5. (Color online) Theoretical simulations of $I(\alpha_i)$ curves for two polarizations of light at 633 nm corresponding to three different particle sizes. Scattering is caused by one air scatterer surrounded by core material placed at the core-cladding interface ($m=1/n_{\mathrm{core}}$). Solid lines: parallel polarization (TM); dashed lines: vertical polarization (TE). Calculations have been done for a POF with $n_{\mathrm{core}}=1.49$, $n_{\mathrm{clad}}=1.4036$, and $\rho_{\mathrm{core}}=490$ μm.

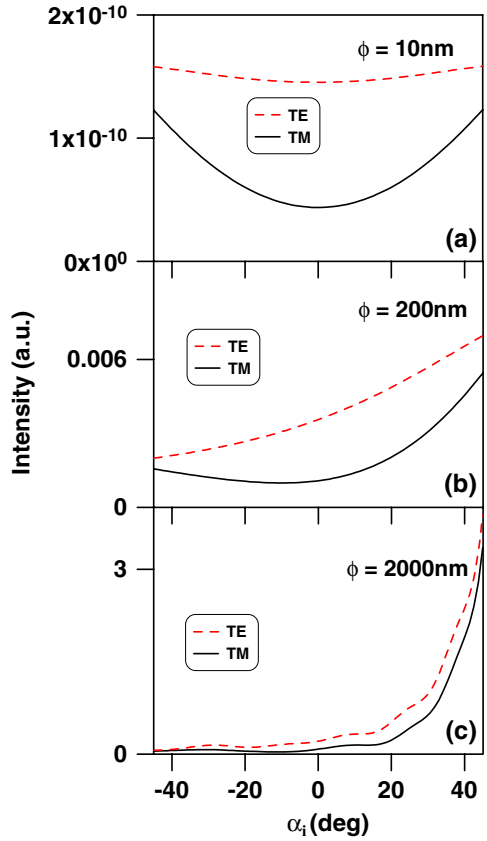

Fig. 6. (Color online) Theoretical simulations of $I(\alpha_i)$ curves for two polarizations of light at 633 nm corresponding to three different particle sizes. Scattering is caused by one cladding scatterer surrounded by core material placed at the core-cladding interface ($m = n_{clad}/n_{core}$). Solid lines: parallel polarization (TM); dashed lines: vertical polarization (TE). Calculations have been done for a POF with $n_{core} = 1.49$, $n_{clad} = 1.4036$ and $\rho_{core} = 490$ μm.

mentioned before, the angular dependence curve corresponding to the cladding sphere shows a lower increase of the intensity at one side of the curve (positive angles) than that corresponding to the air sphere [see Figs. 5(c) and 6(c)]. This lower slope is closer to the experimental behavior detected. On the other hand, in agreement with the experimental measurements, we can see that the $I(y_P)$ curves for both polarizations in Figs. 8(b) and 8(c) do not practically vary with y_P, excluding the two peaks emerging at the boundaries of the core-cladding interface. Notice that this behavior is not observed in the $I(y_P)$ curves calculated for the air sphere [see Figs. 7(b) and 7(c)]. If we try to fit the experimental $I(\alpha_i)$ and $I(y_P)$ curves to theoretical curves calculated for one cladding sphere, the obtained result, though acceptable, is not as good as it could be expected. As an example, we show in Fig. 9 an experimental $I(\alpha_i)$ curve and theoretical simulations calculated at several sizes of the cladding scatterer placed at the core-cladding interface and surrounded by core material. The experimental curve is the $I(\alpha_i)$ curve for parallel polarization corresponding to PGU-CD1001-22-E step-index POF from Toray [16]. The theoretical curves have been normalized to the experimental curve at $\alpha_i = 0$. Although the theoretical simulations describe in general the shape of the experimental curve, there is not a good agreement at the boundaries of the representation range. The best result is obtained for a scatterer size of around $\phi = 300 \pm 50$ nm. The confidence level for the scatterer size (50 nm) is determined by the scatterer size step used in the simulations. Similarly, in Fig. 10 we can see the experimental $I(y_P)$ curve for vertical polarization corresponding to the PGU-CD1001-22-E step-index POF [16] together with the theoretical simulations calculated at several sizes of the cladding scatterer normalized to the experimental curve at $y_P = 0$. The asymmetry observed in the intensity peaks of the experimental curve are attributed to fiber irregularities and to tolerances in the diameters of the fiber's core and cladding. As it can be observed, the theoretical simulations do not describe properly the increase from the center ($y_P = 0$) towards the boundaries of the peaks or the asymmetry of the intensity peaks, obviously. The best result is obtained for a scatterer size of around $\phi = 750 \pm 50$ nm. Similar size range is estimated by fitting the $I(\alpha_i)$ and $I(y_P)$ experimental curves of this fiber corresponding to the other polarizations (250 nm–800 nm). The analysis performed in another step-index fiber, Super ESKA SK-40 POF from Mitsubishi [16], gives also similar results.

In the previous analysis, we must take into account that only one cladding scatterer placed at the core-cladding interface is being considered and that there may be other

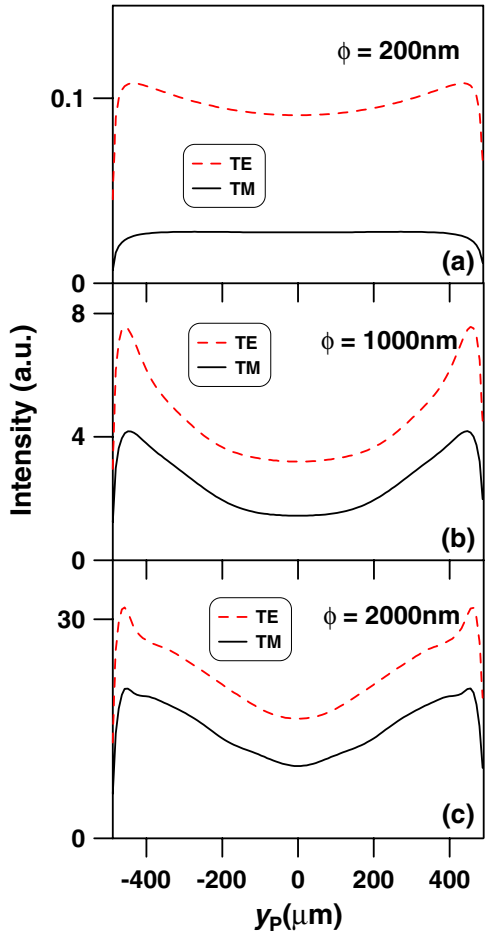

Fig. 7. (Color online) Theoretical simulations of $I(y_P)$ curves for two polarizations of light at 633 nm corresponding to three different particle sizes. Scattering is caused by one air scatterer surrounded by core material placed at the core-cladding interface ($m = 1/n_{core}$). Solid lines: parallel polarization (TM); dashed lines: vertical polarization (TE). Calculations have been done for a POF with $n_{core} = 1.49$, $n_{clad} = 1.4036$, and $\rho_{core} = 490$ μm.

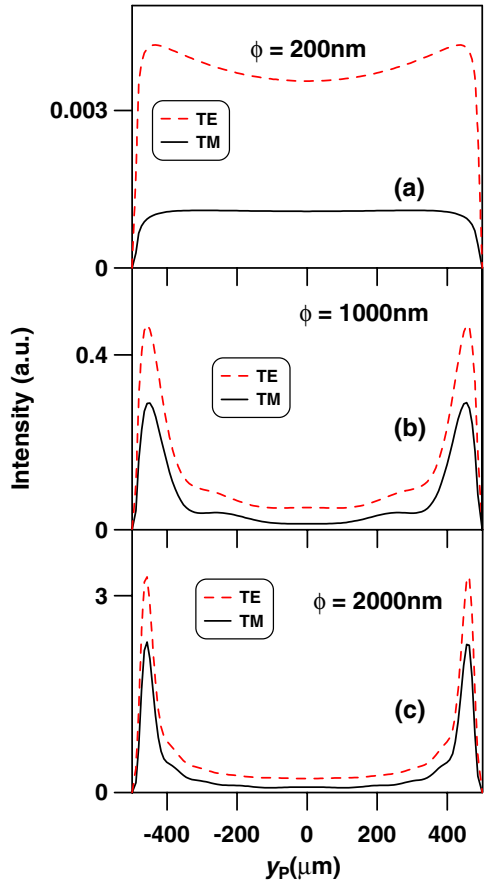

Fig. 8. (Color online) Theoretical simulations of $I(y_P)$ curves for two polarizations of light at 633 nm corresponding to three different particle sizes. Scattering is caused by one cladding scatterer surrounded by core material placed at the core-cladding interface ($m = n_{clad}/n_{core}$). Solid lines: parallel polarization (TM); dashed lines: vertical polarization (TE). Calculations have been done for a POF with $n_{core} = 1.49$, $n_{clad} = 1.4036$, and $\rho_{core} = 490$ μm.

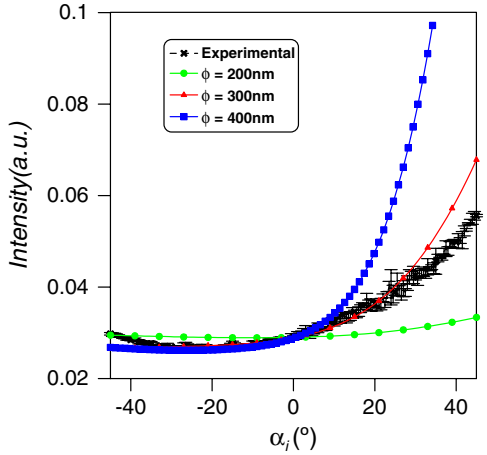

Fig. 9. (Color online) Theoretical simulations of $I(\alpha_i)$ curves for TM polarization of light at 633 nm corresponding to different particle sizes. Scattering is caused by one cladding scatterer surrounded by core material placed at the core-cladding interface ($m = n_{clad}/n_{core}$). Calculations have been done for a POF with $n_{core} = 1.49$, $n_{clad} = 1.4036$, and $\rho_{core} = 490$ μm. The experimental result corresponds to the curve for parallel polarization of Fig. 5(a) in [16].

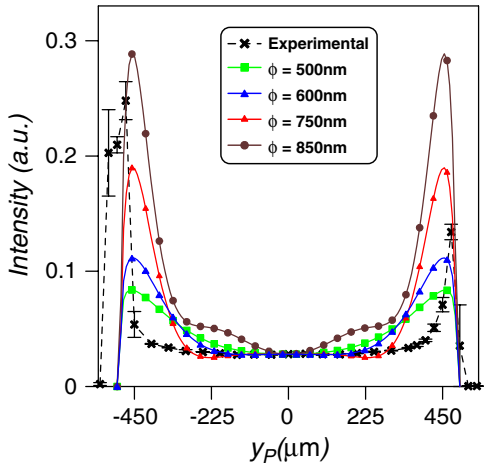

Fig. 10. (Color online) Theoretical simulations of $I(y_P)$ curves for TE polarization of light at 633 nm corresponding to different particle sizes. Scattering is caused by one cladding scatterer surrounded by core material placed at the core-cladding interface ($m = n_{clad}/n_{core}$). Calculations have been done for a POF with $n_{core} = 1.49$, $n_{clad} = 1.4036$, and $\rho_{core} = 490$ μm. The experimental result corresponds to the curve for vertical polarization of Fig. 4(a) in [16].

scatterers within the fiber which can affect the experimental results. However, calculations performed by considering air scatterers or scatterers of cladding material distributed within the core do not improve the above results. The scattered curves obtained in this case for the two types of scatterer at two sizes, $\phi = 500$ nm and $\phi = 2000$ nm, are plotted in

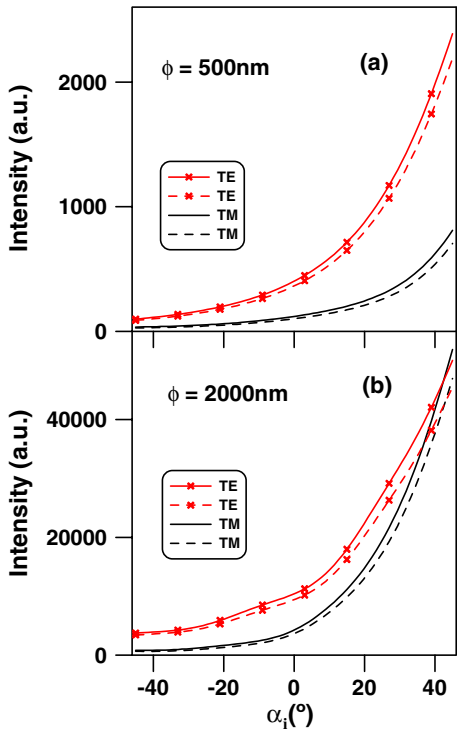

Fig. 11. (Color online) Theoretical simulations of $I(\alpha_i)$ curves for two polarizations of light at 633 nm corresponding to two different particle sizes. Scattering is caused by air scatterers within the core ($m = 1/n_{core}$). Calculations have been done for a POF with $n_{core} = 1.49$, $n_{clad} = 1.4036$, and $\rho_{core} = 490$ μm. Lines with symbols: vertical polarization (TE). Lines without symbols: parallel polarization (TM). Solid lines: using Eq. (5). Dashed lines: using Eq. (12).

Figs. 11–14. It can be observed, for example, that the curves corresponding to each polarization are more distant, that is, differ more in their values. This indicates that the disagreement between the theory and the experimental results is now larger than that obtained for one scatterer at core-cladding interface (see Figs. 4 and 5 in [16]). It must be remarked that the probability of having large inhomogeneities within the core fiber is expected to be low in commercial fibers. The effects of changing the placement of a single scattering sphere, from the core/cladding interface to the core region of the fiber, are particularly noticeable in the near- and far-field patterns [16]. The comparison of computer simulations with the experimentally detected near- and far-field patterns also indicates that the most influential inhomogeneities that give rise to the scattering in POFs are placed at the interface between the core and the cladding [16]. In summary, we have demonstrated that the application of the proposed model can help to describe how is the dominant scattering effect occurring in the fibers. Particularly, we have shown that the main source of the scattering produced in the commercial step-index POFs analyzed is a cladding inhomogeneity placed at the core-cladding interface with a mean size in the range between 200 nm and 850 nm.

We must remark that all of our calculations have been performed by taking into account the accurate expression derived for the maximum angle of acceptance inside the fiber. As an example of this fact, we have plotted in Figs. 11 and 12 the curves of the scattered intensity as a function of the incident angle for both polarizations obtained for air scatterers and scatterers of cladding material within the core calculated by using the exact integral [Eq. (5)] and by using the following approximate integral (Fig. 2 shows the selected integration region):

$$I_{\mathrm{TE,TM}}(\alpha_i) \propto T_{\mathrm{TE,TM}}(\alpha_i) \int_0^{2\pi} \mathrm{d}\phi_x \int_{-n\rho_{\mathrm{core}}}^{n\rho_{\mathrm{core}}} \frac{\mathrm{d}x_Q}{\cos\,\alpha_r} \int_0^{(\theta_z)_c(x_Q,\phi_x)} \times F(\theta_z,\phi_x)|_{\mathrm{TE,TM}}\,\sin\,\theta_z \mathrm{d}\theta_z. \quad (12)$$

With the exception of the integration limits of the second integral, a similar expression to the above one was used in Eqs. (21) and (22) of [14]. This integral represents the scattered intensity by neglecting the contribution of some tunneling rays, particularly those with a high critical angle. On the assumption that the propagation losses of both guided and tunneling rays are negligible we can analyze how the scattered curves change if we use this approach. As it can be observed (see Figs. 11 and 12) the shape of the curves hardly changes and the main difference between the curves obtained from Eq. (5) and from Eq. (12) is the scattered intensity value. At $\alpha_i = 0$, the relative difference between two calculations is around 17% for the TM polarization curve and 9% for the TE polarization one. Similarly, in Figs. 13 and 14 we show the curves of the scattered intensity as a function of the lateral height for air scatterers and scatterers of cladding material

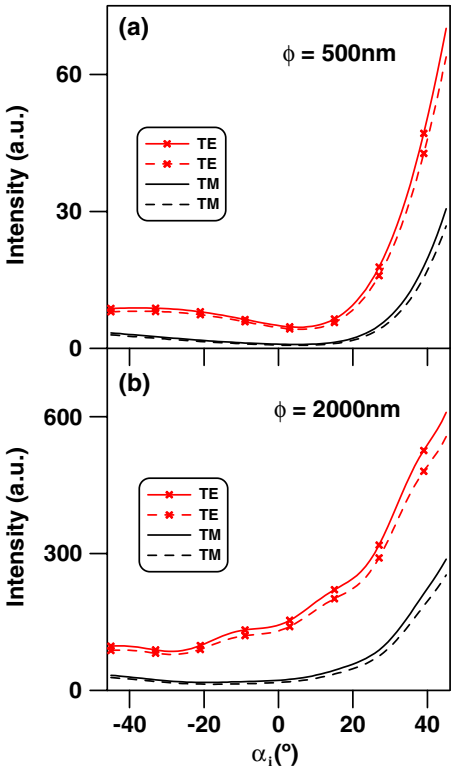

Fig. 12. (Color online) Theoretical simulations of $I(\alpha_i)$ curves for two polarizations of light at 633 nm corresponding to two different particle sizes. Scattering is caused by cladding material scatterers within the core ($m = n_{\mathrm{clad}}/n_{\mathrm{core}}$). Calculations have been done for a POF with $n_{\mathrm{core}} = 1.49$, $n_{\mathrm{clad}} = 1.4036$, and $\rho_{\mathrm{core}} = 490\ \mu$m. Lines with symbols: vertical polarization (TE). Lines without symbols: parallel polarization (TM). Solid lines: using Eq. (5). Dashed lines: using Eq. (12).

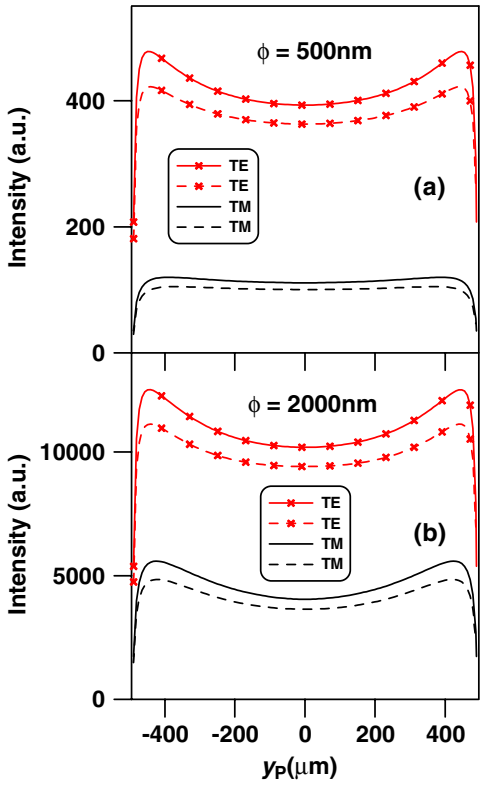

Fig. 13. (Color online) Theoretical simulations of $I(y_P)$ curves for two polarizations of light at 633 nm corresponding to two different particle sizes. Scattering is caused by air scatterers within the core ($m = 1/n_{\mathrm{core}}$). Calculations have been done for a POF with $n_{\mathrm{core}} = 1.49$, $n_{\mathrm{clad}} = 1.4036$, and $\rho_{\mathrm{core}} = 490\ \mu$m. Lines with symbols: vertical polarization (TE). Lines without symbols: parallel polarization (TM). Solid lines: using Eq. (9). Dashed lines: using Eq. (13).

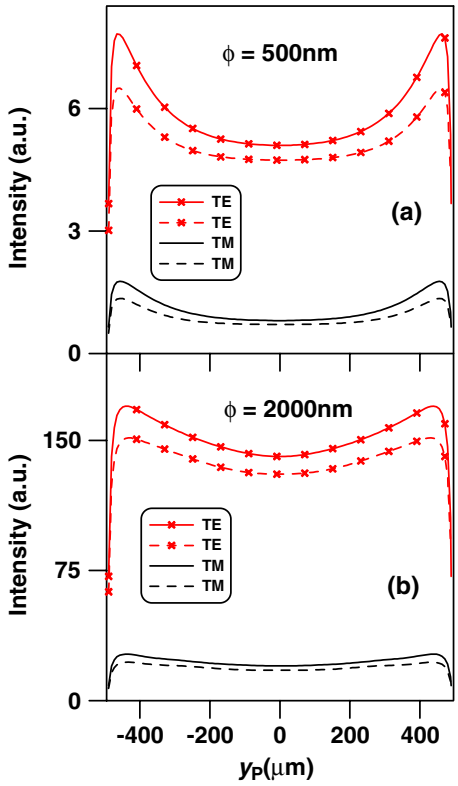

Fig. 14. (Color online) Theoretical simulations of $I(y_P)$ curves for two polarizations of light at 633 nm corresponding to two different particle sizes. Scattering is caused by cladding material scatterers within the core ($m = n_{\text{clad}}/n_{\text{core}}$). Calculations have been done for a POF with $n_{\text{core}} = 1.49$, $n_{\text{clad}} = 1.4036$, and $\rho_{\text{core}} = 490\ \mu$m. Lines with symbols: vertical polarization (TE). Lines without symbols: parallel polarization (TM). Solid lines: using Eq. (9). Dashed lines: using Eq. (13).

within the core obtained by using the exact integral calculation [Eq. (9)] and by using this approximate integral [see Eq. (7) to deduce the selected integration region]:

$$I_{\text{TE,TM}}(y_P) \propto T_{\text{TE,TM}}(y_P) \int_{-\sqrt{\rho_{\text{core}}^2 n^2 - (y_P/n_{\text{core}})^2}}^{\sqrt{\rho_{\text{core}}^2 n^2 - (y_P/n_{\text{core}})^2}} \mathrm{d}x'_Q \int_0^{2\pi} \mathrm{d}\phi_x \times \int_0^{(\theta_z)_c(x'_Q,\phi_x,y_P)} F(\theta_z,\phi_x)|_{\text{TE,TM}} \sin\theta_z \mathrm{d}\theta_z. \quad (13)$$

As before, this integral is the scattered intensity from the fiber by neglecting the contribution of some tunneling rays. If we compare the scattered intensity curves the main difference between them is again the value of the scattered intensity (see Figs. 13 and 14). At $y_P = 0$, the relative difference between two calculations is around 12% for the TM polarization curve and 7% for the TE polarization one. A similar expression to Eq. (13) was used in Eqs. (12) and (13) of [14] excluding the integration limits of the second integral. Notice that the differences between both calculations would be more noticeable if the value of $n = n_{\text{clad}}/n_{\text{core}}$ were lower.

4. SUMMARY

We have worked out a theoretical model which describes the generation of scattered light when step-index polymer optical fibers are transversally illuminated. Specifically, the model describes the dependence of the scattered light intensity on different launching conditions. The theory has been developed using the Mie theory for spheres in the independent-scatterer approximation which allows selecting the size and the material of the scatterer, the material surrounding the scatterer, as well as the wavelength of the incident radiation and its polarization. The application of this theory to experimental measurements can be useful to estimate the size, the nature, and the position of the scatterers in fibers.

APPENDIX A: MAXIMUM ACCEPTANCE ANGLE (ANGULAR DEPENDENCE)

Figure 15 shows the geometrical arrangement corresponding to the side incidence used on the fiber, together with the definition of the angles used for the theoretical analysis. The incident beam refracts at the interface point ($P(\rho_{\text{core}}, 0, z)$) from the air to the fiber. **i**, **r**, and **n** are the unit vectors denoting the directions of the incident light, the refracting light, and the normal to the interface at point P, respectively. These are expressed as

$$\mathbf{i} = -\cos\alpha_i \mathbf{x} + \sin\alpha_i \mathbf{z}, \quad \mathbf{r} = -\cos\alpha_r \mathbf{x} + \sin\alpha_r \mathbf{z}, \quad n = x. \quad (A1)$$

Consequently, the xz plane is the plane of incidence and, therefore, α_i and α_r are the incident and the refracting angles [see Figs. 15(a) and 15(b)]. From Snell's law, we have:

$$\sin\alpha_r = \frac{\sin\alpha_i}{n_{\text{clad}}}, \quad (A2)$$

with n_{clad} the refractive index of the fiber cladding. At the point P on the interface, the incident beam suffers attenuation given by Fresnel's coefficients which depend on the refractive indexes of the first medium ($n_i = 1$) and the second one ($n_t = n_{\text{clad}}$) and also on the angle of incidence (α_i). Two polarizations of the incident light have been analyzed: vertical to the incident plane (TE) and parallel (TM). In our case, for TE polarization the electric field **E** of the incident beam is directed along y-axis, while for TM polarization it lies on the xz plane. The Fresnel's coefficients as a function of α_i for these polarizations are expressed as

$$T_{\text{TE}}(\alpha_i) = \frac{4\cos\alpha_i \sqrt{n_{\text{clad}}^2 - \sin^2\alpha_i}}{\left(\cos\alpha_i + \sqrt{n_{\text{clad}}^2 - \sin^2\alpha_i}\right)^2}, \quad (A3)$$

$$T_{\text{TM}}(\alpha_i) = \frac{4\cos\alpha_i \sqrt{n_{\text{clad}}^2 - \sin^2\alpha_i}}{\left(n_{\text{clad}}\cos\alpha_i + \frac{1}{n_{\text{clad}}}\sqrt{n_{\text{clad}}^2 - \sin^2\alpha_i}\right)^2}. \quad (A4)$$

By assuming that the scattered beam is produced at any point Q of the refracted beam inside the fiber, the direction of one arbitrary scattered beam from that point $Q(x_Q, 0, z)$ is expressed by the unit vector **s** as follows:

$$\mathbf{s} = \sin\theta_z \cos\phi_x \mathbf{x} - \sin\theta_z \sin\phi_x \mathbf{y} + \cos\theta_z \mathbf{z}. \quad (A5)$$

θ_z is the angle taken by **s** with respect to the fiber axis (z-axis), whereas ϕ_x describes the angle of **s** relative to the x-axis in the xy-plane [see Fig. 15(c)]. Some of the scattered light will refract out from the fiber and the rest will be guided forward

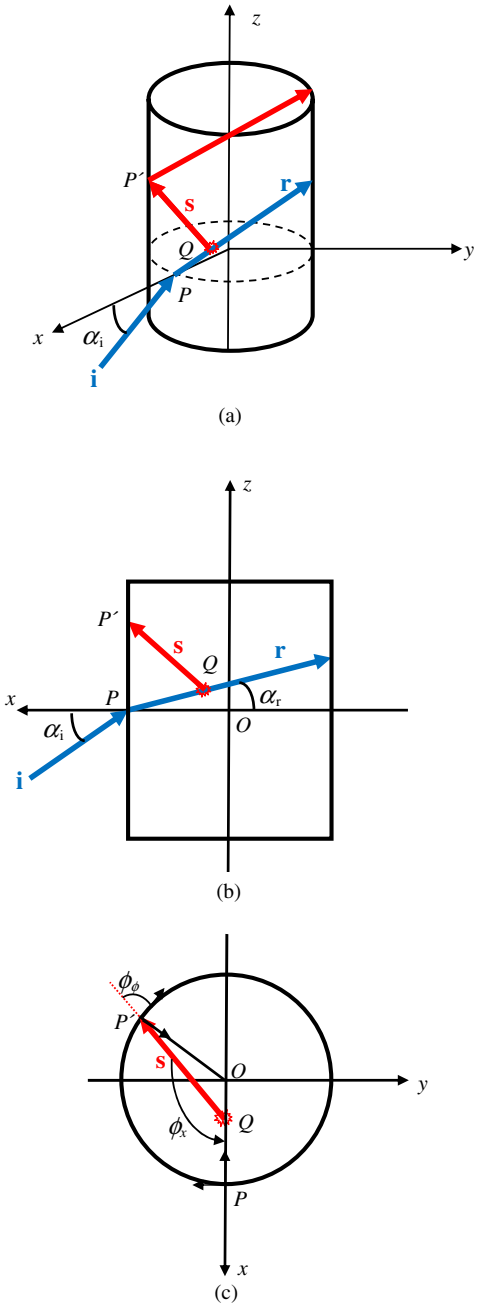

Fig. 15. (Color online) (a) and (b) Geometrical arrangement of the POF with respect to the incident beam for angular scanning. α_i is the angle made by the incident beam with the normal to the fiber surface at $y = 0$ μm. The incident beam **i** always lies in the xz-plane. **s** represents the scattered beam, while **r** the refracted beam. (c) Definition of angles used for theoretical analysis.

and backward to both fiber ends. The light scattered from point Q strikes at point P' at the core-cladding interface (see Fig. 15). If total internal reflection occurs, the following equation is satisfied:

$$\sin \alpha_c = \frac{n_{\text{clad}}}{n_{\text{core}}}. \tag{A6}$$

Here α_c is the critical angle with respect to the normal at P'. n_{core} is the refractive index of the fiber core. In order to calculate the critical angle with respect to the fiber axis, $(\theta_z)_c$, we use the next expression:

$$\sin (\theta_z)_c = \frac{\cos \alpha_c}{\sin \phi_\phi}, \tag{A7}$$

where ϕ_ϕ is the angle in the core cross-section between the tangent to the interface at P' and the projection of **s** [see Fig. 15(c)]. The relation between ϕ_ϕ and ϕ_x is found by geometry to be

$$\cos \phi_\phi = \frac{x_Q}{\rho_{\text{core}}} \sin \phi_x. \tag{A8}$$

By inserting Eqs. (A6) and (A8) into Eq. (A7), we obtain the following expression for the critical angle corresponding to the scattered beam emerging from the point $Q(x_Q, 0, z)$:

$$\begin{aligned} \sin (\theta_z)_c(x_Q, \phi_x) &= \frac{\sqrt{1 - \left(\frac{n_{\text{clad}}}{n_{\text{core}}}\right)^2}}{\sin\left(\arccos\left(\frac{x_Q}{\rho_{\text{core}}} \sin \phi_x\right)\right)} \\ &= \frac{\sqrt{1 - n^2}}{\sqrt{1 - \left(\frac{x_Q}{\rho_{\text{core}}} \sin \phi_x\right)^2}}. \end{aligned} \tag{A9}$$

n represents the quotient $n_{\text{clad}}/n_{\text{core}}$. If the scattered light were produced from one scatterer placed just at the core-cladding interface of the fiber, x_Q would be equal to the radius of the fiber ρ_{core}, so that the critical angle could be simplified as

$$\sin (\theta_z)_c(\rho_{\text{core}}, \phi_x) = \frac{\sqrt{1 - n^2}}{\sqrt{1 - (\sin \phi_x)^2}} = \frac{\sqrt{1 - n^2}}{\cos \phi_x}. \tag{A10}$$

APPENDIX B: MAXIMUM ACCEPTANCE ANGLE (LATERAL DEPENDENCE)

Figure 16 shows the geometrical arrangement corresponding to this launching condition together with the definition of the angles used for the theoretical analysis. In this case, **i** and **r**, the unit vectors indicating the directions of the incident and refracting light, respectively, are written as

$$\mathbf{i} = -\mathbf{x}, \quad \mathbf{r} = -\cos(\alpha_i - \alpha_r)\mathbf{x} - \sin(\alpha_i - \alpha_r)\mathbf{y}. \tag{B1}$$

As a result, the incident plane is now the xy-plane. The refraction of the incident beam takes place at point $P(x, y, z)$ of the interface and Snell's law is expressed as

$$\begin{aligned} &\sin \alpha_r = \frac{\sin \alpha_i}{n_{\text{clad}}}, \quad \text{with} \quad \alpha_i = \arctan\left(\frac{y_P}{x_P}\right) \quad \text{and} \\ &\rho_{\text{core}} = \sqrt{x_P^2 + y_P^2}. \end{aligned} \tag{B2}$$

The Fresnel's coefficients for the polarizations considered in this study are now expressed as a function of y_P as follows:

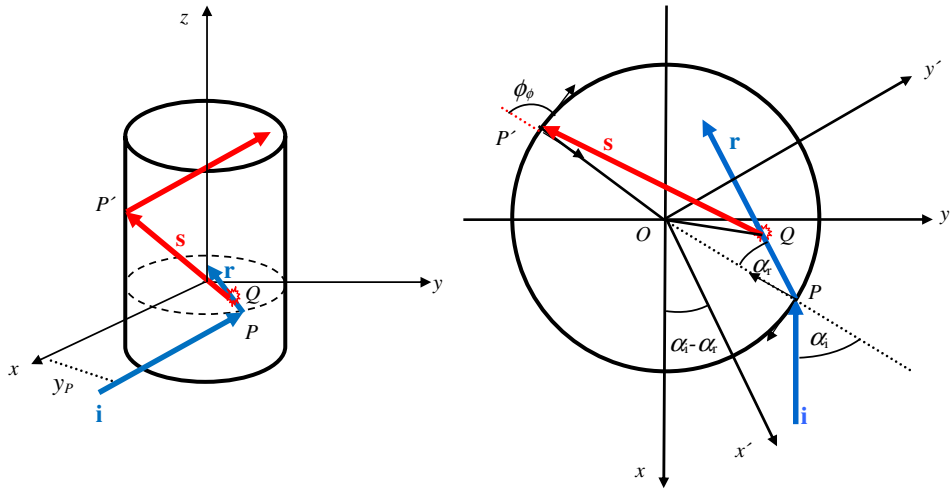

(a) (b)

Fig. 16. (Color online) (a) Geometrical arrangement of the POF with respect to the incident beam for lateral scanning. y_P refers to the y-coordinate of the point of incidence relative to $y = 0$ μm. The incident beam always lies in the xy-plane (parallel to the x-axis). **s** represents the scattered beam, while **i** and **r**, the incident and refracted beams. (b) Definition of angles used for theoretical analysis.

$$T_{\mathrm{TM}}(y_P) = \frac{4\sqrt{\rho_{\mathrm{core}}^2 - y_P^2}\sqrt{\rho_{\mathrm{core}}^2 n_{\mathrm{clad}}^2 - y_P^2}}{\left(n_{\mathrm{clad}}\sqrt{\rho_{\mathrm{core}}^2 - y_P^2} + \frac{1}{n_{\mathrm{clad}}}\sqrt{\rho_{\mathrm{core}}^2 n_{\mathrm{clad}}^2 - y_P^2}\right)^2}, \quad \text{(B3)}$$

$$T_{\mathrm{TE}}(y_P) = \frac{4\sqrt{\rho_{\mathrm{core}}^2 - y_P^2}\sqrt{\rho_{\mathrm{core}}^2 n_{\mathrm{clad}}^2 - y_P^2}}{\left(\sqrt{\rho_{\mathrm{core}}^2 - y_P^2} + \sqrt{\rho_{\mathrm{core}}^2 n_{\mathrm{clad}}^2 - y_P^2}\right)^2}. \quad \text{(B4)}$$

The direction of the scattered beam from any point Q placed along the refracting beam given by Eq. (A5) is also valid in this case. From Fig. 16(b), θ_z is the angle taken by **s** with respect to the fiber axis (z-axis) and ϕ_x is the angle of **s** relative to the x-axis in the xy-plane. The scattered beam from the point Q strikes at a point P' at the fiber interface; if total internal reflection occurs, the critical angle with respect to the fiber axis is also given by Eq. (A7).

Let us calculate the expression for the critical angle corresponding to any point source Q along the refracting beam in the xy-plane. By applying geometrical rules in the triangle $OP'Q$ [see Fig. 16(b)], we obtain the following relation between the angles ϕ_ϕ and ϕ_x:

$$\cos\phi_\phi = \frac{r}{\rho_{\mathrm{core}}}\sin\left[\phi_x + \arctan\left(\frac{y_Q}{x_Q}\right)\right], \quad \text{with} \quad r = \sqrt{x_Q^2 + y_Q^2}. \quad \text{(B5)}$$

In order to facilitate the integration of the scattered light intensity along the direction of the refracted beam, we rotate the reference system an angle $(\alpha_i - \alpha_r)$ around the z-axis. This way, we obtain a new reference system (x', y', z) with the x'-axis directed along the path covered by the refracted beam. By applying again geometrical rules in the OPQ triangle [see Fig. 16(b)], we obtain the following relation for $\arctan(y_Q/x_Q)$:

$$\begin{aligned}\arctan\left(\frac{y_Q}{x_Q}\right) &= \arctan\left(\frac{y'_Q}{x'_Q}\right) + \alpha_i - \alpha_r \\ &= \arctan\left(\frac{y'_Q}{x'_Q}\right) + \arctan\left(\frac{y_P}{x_P}\right) - \arcsin\left(\frac{\sin\alpha_i}{n_{\mathrm{core}}}\right),\end{aligned} \quad \text{(B6)}$$

with $r = \sqrt{x_Q^2 + y_Q^2} = \sqrt{x_Q'^2 + y_Q'^2}$, $\rho_{\mathrm{core}} = \sqrt{x_P^2 + y_P^2} = \sqrt{x_P'^2 + y_P'^2}$, and $y'_P = y'_Q = \frac{y_P}{n_{\mathrm{core}}}$.

In the above expressions $\sin\alpha_r$ [Eq. (B2)] has been replaced by $\sin\alpha_i/n_{\mathrm{core}}$ in order to describe the direction of the refracted beam along the core fiber. It must be remembered that the thickness of the cladding is neglected. By inserting Eqs. (B5) and (B6) into Eq. (A7), we obtain the expression of the maximum acceptance angle $(\theta_z)_c$ for the scattered beam as a function of three variables: x'_Q, the position of the scatterer along the refracting beam (x'-axis), ϕ_x, the angle relative to the x-axis in the xy-plane, and, y_P, the height of the incident point on the fiber. Thus:

$$\sin(\theta_z)_c(x'_Q, \phi_x, y_P) = \frac{\sqrt{1 - n^2}}{\sin\Delta}, \quad \text{(B7)}$$

with

$$\sin\Delta = \sqrt{1 - \frac{(x'_Q)^2 + \left(\frac{y_P}{n_{\mathrm{core}}}\right)^2}{\rho_{\mathrm{core}}^2}\sin^2\left[\phi_x + \arctan\left(\frac{y_P}{n_{\mathrm{core}}x'_Q}\right) + \arctan\left(\frac{y_P}{\sqrt{\rho_{\mathrm{core}}^2 - y_P^2}}\right) - \arcsin\left(\frac{y_P}{\rho_{\mathrm{core}}n_{\mathrm{core}}}\right)\right]}.$$

If the scattering center is placed at the core-cladding interface, $\rho_{\text{core}} = \sqrt{x_Q^2 + y_Q^2} = \sqrt{x_Q'^2 + y_Q'^2}$, Eq. (B7) is simplified to

$$\sin(\theta_z)_c(\phi_x, y_P) = \frac{\sqrt{1-n^2}}{\cos\left[\phi_x + \arctan\left(\frac{y_P}{\sqrt{\rho_{\text{core}}^2 - y_P^2}}\right)\right]}, \qquad \text{(B8)}$$

Notice that, if y_P were 0, that is, if $\alpha_i = 0$, Eqs. (B7) and (B8) would be simplified to Eqs. (A9) and (A10), respectively.

ACKNOWLEDGMENTS

This work was supported by the institutions Ministerio de Ciencia e Innovación, Gobierno Vasco/Eusko Jaurlaritza, and Diputación Foral de Bizkaia/Bizkaiko Foru Aldundia, under projects TEC2009-14718-C03-01 and COBOR, GIC07/156-IT-343-07, AIRHEM-II, S-PR10UN04, S-PE09CA03 and DENSHIA, and 06-12-TK-2010-0022, respectively. The research leading to these results has also received funding from the European Commission's Seventh Framework Programme (FP7) under grant agreement no. 212912 (AISHA II). This work has been created in the Training and Research Unit UFI11/16 supported by the University of the Basque Country (UPV/EHU).

REFERENCES

1. J. Zubia and J. Arrue, "Plastic optical fibers: an introduction to their technological processes and applications," Opt. Fiber Technol. **7**, 101–140 (2001).
2. T. Kaino, "Polymer optical fibers," in *Polymers for Lightwave and Integrated Optics* (Marcel Dekker, 1992), Chap. 1.
3. O. Ziemann, J. Krauser, P. E. Zamzow, and W. Daum, *POF Handbook: Optical Short Range Transmission Systems*, 2nd ed. (Springer, 2008).
4. D. Kalymnios, P. Scully, J. Zubia, and H. Poisel, "POF sensors overview," in *Proceedings of the 13th International Plastic Optical Fibres Conference*, (Nürnberg, Germany, 2004), 237–244.
5. M. C. J. Large, D. Blacket, and C. A. Bunge, "Microstructured polymer optical fibers compared to conventional POF: novel properties and applications," IEEE Sensors Journal **10**, 1213–1217 (2010).
6. J. Clark and G. Lanzani, "Organic photonics for communications," Nature Photonics **4**, 438–446 (2010).
7. G. V. Maier, T. N. Kopylova, V. A. Svetlichnyi, V. M. Podgaetskii, S. M. Dolotov, O. V. Ponomareva, A. E. Monich, and E. A. Monich, "Active polymer fiebers doped with organic dyes: generation and amplification of coherent radiation," Quantum Electron. **37**, 53–59 (2007).
8. M. Sheeba, K. J. Thomas, M. Rajesh, V. P. N. Nampoori, C. P. G. Vallabhan, and P. Radhakrishnan, "Multimode laser emission from dye doped polymer optical fiber," Appl. Opt. **46**, 8089–8094 (2007).
9. M. A. Illarramendi, J. Zubia, L. Bazzana, G. Durana, G. Aldabaldetreku, and J. R. Sarasua, "Spectroscopic characterization of plastic optical fibers doped with fluorene oligomers," J. Lightwave Technol. **27**, 3220–3226 (2009).
10. D. Gloge, "Optical power flow in multimode fibers," Bell Syst. Tech. J. **51**, 1767–1783 (1972).
11. A. W. Snyder and J. D. Love, *Optical Waveguide Theory* (Chapman and Hall, 1983).
12. Y. Koike, N. Tanio, and Y. Ohtsuka, "Light scattering and heterogeneities in low-loss poly(methyl methacrylate) glasses," Macromolecules **22**, 1367–1373 (1989).
13. Y. Koike, S. Matsuoka, and H. E. Bair, "Origin of excess light scattering in poly(methyl methacrylate) glasses," Macromolecules **25**, 4807–4815 (1992).
14. C. A. Bunge, R. Kruglov, and H. Poisel, "Rayleigh and Mie scattering in polymer optical fibers," J. Lightwave Technol. **24**, 3137–3146 (2006).
15. M. G. Kuzyk, *Polymer Fiber Optics: Materials, Physics, and Applications* (Taylor and Francis, 2007).
16. G. Aldabaldetreku, I. Bikandi, M. A. Illarramendi, G. Durana, and J. Zubia, "A comprehensive analysis of scattering in polymer optical fibers," Opt. Express **18**, 24536–24555 (2010).
17. H. C. van de Hulst, *Light Scattering by Small Particles* (Dover, 1981).
18. M. I. Mishchenko, L. D. Travis, and A. A. Lacis, *Scattering, Absorption and Emission of Light by Small Particles* (Cambridge University, 2002).
19. M. J. Adams, *An Introduction to Optical Waveguide*, (John Wiley, 1981).
20. M. Kerker, *The Scattering of Lght and Other Electromagnetic Radiation* (Academic, 1969).
21. C. F. Bohren and D. R. Huffman, *Absorption and Scattering of Light by Small Particles* (John Wiley, 1983).